Stabilization of the Current-Driven Electrostatic Ion-Cyclotron Instability by Lower-Hybrid Waves

N. S. Wolf,[a] R. Majeski, and H. Lashinsky[b]
Institute for Physical Science and Technology, University of Maryland, College Park, Maryland 20742

and

V. Tripathi and C. S. Liu
Department of Physics and Astronomy, University of Maryland, College Park, Maryland 20742
(Received 24 October 1979)

The current-driven electrostatic ion-cyclotron instability in a Q machine operated in the low-density regime $(\omega_{pe}/\omega_{ce})^2 \ll 1$ is stabilized by externally generated rf electrostatic fields in the lower-hybrid range. Stabilization is due to a resonant ponderomotive force, which reduces the instability frequency, thus increasing the ion-cyclotron damping. The experimental results are in good agreement with an analysis which describes the effect of rf power on the instability frequency shift and growth rate.

PACS numbers: 52.35.Mw, 52.35.Fp, 52.35.Py

Under appropriate conditions the nonlinear interaction between a high-frequency (Ω) electrostatic field and a low-frequency (ω) electrostatic plasma instability ($\Omega \gg \omega$) can be used to suppress the instability.[1-3] The high-frequency pump field E_Ω produces a high-frequency oscillatory electron velocity v_Ω and the nonlinear interaction between v_Ω and n_ω, the low-frequency density fluctuation associated with the instability, generates high-frequency sideband electrostatic fields. These fields beat with E_Ω to produce a ponderomotive force $F_{p\omega}$ at the instability frequency. Depending on its phase, $F_{p\omega}$ either increases or decreases the instability frequency, $\omega \to \omega \pm \Delta\omega$; if the instability is subject to a frequency-dependent damping mechanism, and if $\Delta\omega$ is of the proper sign and magnitude, the instability can be stabilized. In general, E_Ω is conveniently introduced by exciting a passive, high-frequency, electrostatic plasma resonance with an external source.[4] This stabilization method is closely related to a technique known as "dither stabilization" in control engineering.[5]

The effects of the ponderomotive force in the stabilization of the collisionless drift wave have been demonstrated experimentally by using electrostatic fields in the lower-hybrid range of frequencies.[6] In the present work, lower-hybrid waves are used to demonstrate the suppression of the current-driven electrostatic ion-cyclotron instability,[7-10] an important instability recently observed in tokamaks[11] and over the auroral zone of the magnetosphere.[12] The lower-hybrid wave can cause a nonlinear frequency shift of the ion-cyclotron mode, thus reducing $\omega - \omega_{ci}$ and causing a corresponding increase of the ion-cyclotron damping; this process leads to stabilization if the amplitude of the lower-hybrid wave is sufficiently large.

In the analysis we consider a cylindrical plasma with equilibrium density n_0 in a uniform magnetic field $B\hat{z}$; a current $j = nev_d\hat{z}$ flows in the direction of the magnetic field. If $v_d > v_\Phi$, where v_Φ is the parallel phase velocity, the plasma is unstable against the electrostatic ion-cyclotron instability,[7-10] which produces a density perturbation $n_\omega = n_\omega{}^0 \exp[i(\omega t - \vec{k}\cdot\vec{r})]$, where $\omega \gtrsim \omega_{ci}$, the ion-cyclotron frequency. An external source is used to excite an electrostatic (lower-hybrid) standing wave[4] $\vec{E}_\Omega = \vec{E}_\Omega{}^0 \sin(\vec{K}\cdot\vec{r}) \sin\Omega t = -\nabla\Phi_\Omega$, where $\Omega \approx \Omega_{LH}$, the lower-hybrid frequency. This wave field, in turn, generates an oscillatory electron velocity $\vec{V}_\Omega = \vec{V}_\Omega{}^0 \sin(\vec{K}\cdot\vec{r}) \sin\Omega t$. In these experiments $(\omega_{pe}/\omega_{ce}) \ll 1$, so that $\Omega_{LH} \approx (K_z/K)\omega_{pe}$, where ω_{pe} and ω_{ce} are, respectively, the electron plasma and cyclotron frequencies. The electron equation of motion then yields the transverse velocity $V_{\Omega\perp} = \Phi_\Omega K_\perp (e/m)/\omega_{ce}$ and the parallel velocity $V_{\Omega z} = \Phi_\Omega K_z (e/m)\Omega$, in which case $V_{\Omega\perp}/V_{\Omega z} \approx \omega_{pe}/\omega_{ce} \ll 1$ and the transverse velocity can be neglected.

The nonlinear interaction[13,14] between $\vec{V}_\Omega$ and n_ω generates density perturbations at sideband frequencies $n_\pm = (\vec{K}_\pm \cdot \vec{V}_\Omega n_\omega)/2\Omega_\pm$, where the symbol $\vec{K}_\pm$ means $(\vec{K} \pm \vec{k})$, $\Omega_\pm$ means $\Omega \pm \omega$, and $n_\pm = n(K_\pm, \Omega_\pm)$. In turn, the density sidebands produce sideband potentials through the high-frequency Poisson equation, these high-frequency potentials being given by

$$\Phi_\pm = -(4\pi e/k_\pm{}^2)(K_{z\pm} V_\Omega / 2\Omega_\pm \epsilon_\pm) n_\omega, \tag{1}$$

where $\epsilon_\pm \cong 1 - \omega_{pe} K_{z\pm}/\Omega_\pm K_\pm \pm (\omega_*/\Omega)(k\lambda_D)^{-2}$ and ω_*

$= (cT_e/Be)n_0^{-1}dn_0/dx$ is the drift frequency associated with the density gradient. This drift term is found to be small compared with the other terms in $\epsilon_\pm$ and is neglected in the following analysis.

The low-frequency effects of the potentials Φ_Ω, Φ_-, and Φ_+ on the electrons can be described in terms of a *parallel* ponderomotive force[13,14] $F_{p\omega} \equiv -e\partial\varphi_{p\omega}/\partial z = -\frac{1}{2}m(\partial/\partial z)(V_{+z}V_{\Omega z} + V_{-z}V_{\Omega z})$, where $V_{\pm z} = -e\varphi_\pm k_{\pm z}/m\Omega$, and from Eq. (1), $\Phi_{p\omega} = (a/2k_z\lambda_D)^2(T_e/n_0e)\varphi(\Omega)n_\omega$. The coupling parameter $a = k_z eE_{\|\Omega}{}^0/m\Omega^2$ and $\varphi(\Omega)$ is the resonance function

$$\varphi(\Omega) = -\frac{\Omega^2 K_{z+}{}^2}{(\Omega_+ K_+)^2 - (\omega_{pe}K_{z+})^2} - \frac{\Omega^2 K_{z-}{}^2}{(\Omega_- K_-)^2 - (\omega_{pe}K_{z-})^2}. \quad (2)$$

The component of the high-frequency pump wave with $K \to -K$ has been omitted since it only introduces an additive term without affecting the physics. The density perturbation n_ω can also be written in terms of $\Phi_{p\omega}$ through the use of the low-frequency susceptibility: $n_\omega = (k^2/4\pi e)\chi_e(\omega)(\Phi_\omega + \Phi_{p\omega})$. The potential Φ_ω is then determined by using this expression for n_ω in the low-frequency Poisson equation, in which the ion density is given by the usual linear ion susceptibility.[15] This procedure yields the relation $\Phi_\omega = -[\chi_e(\omega)/\epsilon(\omega)] \times \Phi_{p\omega}$, where $\epsilon(\omega) = 1 + \chi_e(\omega) + \chi_i(\omega)$. The expressions for Φ_ω and $\Phi_{p\omega}$ are now used in the relations for n_ω and we obtain the dispersion relation for the current-driven electrostatic ion-cyclotron wave in the presence of the high-frequency field, where the standard expressions[15] are used for $\chi_e(\omega)$ and $\chi_i(\omega)$:

$$1 + a^2\varphi(\Omega)/4(k_z\lambda_D)^2 + b_i + b_i\omega/2(\omega - \omega_{ci}) + i\pi^{1/2}\left\{\frac{\omega - k_z v_d}{k_z v_{Te}} + \frac{b_i\omega_{ci}}{k_z v_{Ti}}\exp\left[\frac{-(\omega-\omega_{ci})^2}{2(k_z v_{Ti})^2}\right]\right\} = 0. \quad (3)$$

This dispersion relation yields the instability frequency

$$\omega = \omega_{ci}\{1 + \tfrac{1}{2}b_i[1 + b_i + \alpha\varphi(\Omega)]^{-1}\} \quad (4)$$

and the growth rate

$$\gamma = \frac{\pi^{1/2}b_i\omega_{ci}}{2^{1/2}[1 + b_i + \alpha\varphi(\Omega)]}\left\{\frac{v_d}{v_{Te}} - \frac{\omega}{k_z v_{Te}} - \frac{\omega - \omega_{ci}}{k_z v_{Ti}}\exp\left[-\frac{(\omega-\omega_{ci})^2}{2(k_z v_{Ti})^2}\right]\right\}, \quad (5)$$

where $\alpha = a^2/4(k_z\lambda_D)^2 = V_{\Omega z}{}^2\omega_{pe}{}^2/2v_{Te}{}^2\Omega^2$, and $b_i = \frac{1}{2}(k_\perp\rho_L)^2$, where ρ_L is the ion Larmor radius.

The three terms in the curly brackets in (5) are recognized as (1) the electron-drift growth term, (2) the electron Landau damping term [first term of the expanded exponential for $\omega/(k_z v_{Te}) \ll 1$], and (3) the ion-cyclotron damping term. When $E = 0$, Eqs. (4) and (5) reduce to the standard expressions for the frequency and growth rate.[7] The saturated amplitude of the instability is proportional to the growth rate.[16] Finally, we note that modifications of the mode structure of the ion-cyclotron instability caused by the lower-hybrid pump have not been included since these should only cause small quantitative changes.[6]

The experiments are carried out in the single-ended collisionless Q-machine plasma configuration described earlier[6] in which the nominal values of the pertinent parameters are as follows: $\omega_{pe} = 5.6\times 10^8$ rad/sec, $\omega_{ci} = 3.9\times 10^5$ rad/sec, $T_e = 0.22$ eV, plasma radius $R = 2$ cm, $\omega_{pe}/\omega_{ce} = 10^{-2}$, $\lambda_D = 3\times 10^{-2}$ cm, $b_i = \frac{1}{2}(k_\perp\rho_L)^2 = 0.48$. A special inductive coupler[4] excites single, discrete lower-hybrid electrostatic modes in which the values of K_z and $K_\perp$ are "quantized" by the finite plasma geometry ($K_z = 0.05$ cm^{-1}). The experiments required a detailed knowledge of the lower-hybrid modes, especially the precise value of Ω_{LH} for a given mode, since the quantity $\Omega - \Omega_{LH}$ in Eq. (2) determines the sign of the ponderomotive force. These modes have been investigated in detail elsewhere.[4]

In the experiments described here we excite a current-driven instability whose frequency, $\omega = 1.16\omega_{ci}$, is found to be proportional to B and independent of k_z; this instability is identified as the electrostatic ion-cyclotron instability. Measurements of the transverse mode structure show $k_\perp \cong 3.5$ cm^{-1}; using the experimental parameters given above and this value of $k_\perp$ in Eq. (4), we find $\omega \cong 1.15\omega_{ci}$, in good agreement with the observed value. These results agree with earlier experimental results on the electrostatic ion-cyclotron instability.[8-10] The experimental procedure then consists of determining the dependence of the instability frequency ω and growth rate γ on the radio-frequency power: $P_{rf} \propto E^2$. For this purpose the applied frequency $\Omega/2\pi$ is kept fixed at 0.82 MHz, in which case it is found that the

ponderomotive force acts to reduce ω. The experiment is performed by increasing the current to a level slightly above the level that corresponds to instability onset with $P_{rf}=0$. The radio-frequency power P_{rf} is then gradually increased from zero and the oscillation frequency ω and steady-state amplitude $A_0=\text{const}\gamma$ are determined as functions of P_{rf}.

The experimental functions $\omega=\omega(P_{rf})$ and $A_0=A_0(P_{rf})$ are conveniently presented as a raster display,[17] in which the current-driven cyclotron mode is observed on a spectrum analyzer. Successive sweeps of the spectrum analyzer are stacked, one above the other (on an auxiliary oscilloscope), while P_{rf} is increased linearly at a slow rate by an electronic ramp circuit, thus forming a display like that in Fig. 1. This figure shows qualitatively the frequency reduction $\Delta\omega$ associated with the E^2 term in Eq. (4) and the associated reduction in amplitude caused by the lower value of ω in the exponential term in Eq. (5).

Quantitative information is presented in Fig. 2, in which is plotted the function $\omega=\omega(P_{rf})$ taken from the raster display in Fig. 1 after preliminary data processing. Evidently $\omega=\omega(P_{rf})$ is a linear function of P_{rf} over almost an order-of-magnitude variation of P_{rf} denoted by the segment I–II in Fig. 2, which is the range of interest. In comparing Eq. (4) with the segment I–II in Fig. 2 we note that the total frequency variation over this interval is small (0.6%), implying that $1\gtrsim b_i \gg\alpha\varphi(\Omega)$. Then Eq. (4) can be expanded and when

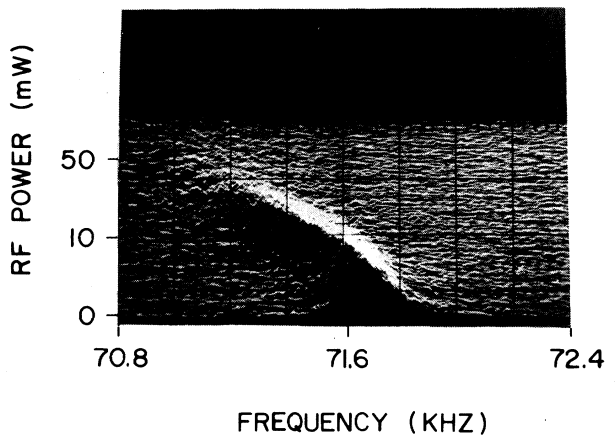

FIG. 1. Raster display (Ref. 17) showing the reduction of the frequency and amplitude of the current-driven ion-cyclotron instability caused by the application of radio-frequency power in the lower-hybrid range of frequencies. The instability signal is derived from fluctuations in the current to the endplate.

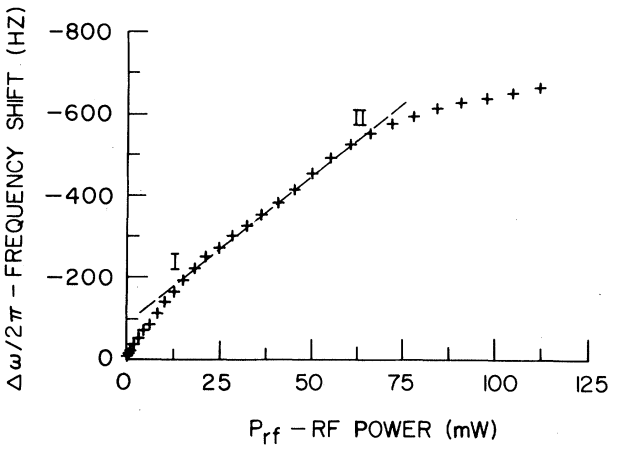

FIG. 2. The frequency of the current-driven ion-cyclotron instability as a function of P_{rf}, the rf power in the lower-hybrid range. The present discussion is concerned with the segment I–II, in which the experimental points lie reasonably close to a straight line. The saturation effect beyond II is not considered here.

the appropriate numerical values are substituted we find the expression $\omega\approx\omega_{ci}[1.16-b_i\alpha\varphi(\Omega)/2(1+b_i)^2]$. The fact that the experimental function $\omega=\omega(P_{rf})$ is linear verifies the linear scaling predicted by Eq. (4).

In Fig. 3 the steady-state amplitude A_0 is plotted as a function of $\Delta\omega$, the frequency shift in Fig. 2; the points marked I and II correspond on the two figures. The solid curve represents a

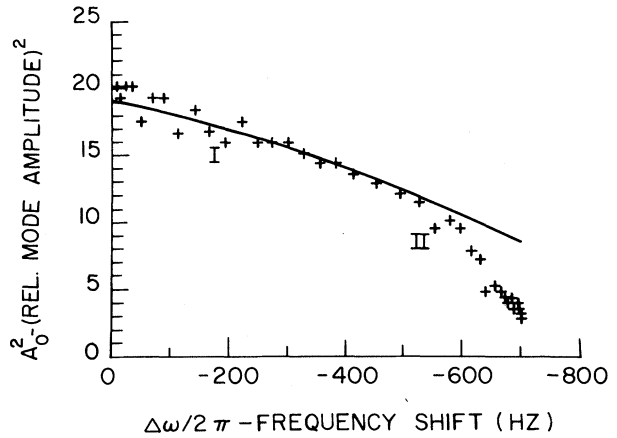

FIG. 3. Steady-state amplitude of the current-driven ion-cyclotron instability as a function of the frequency shift in Fig. 2. The solid curve is a one-point fit to the theory as given in Eq. (5). The scatter in the experimental points to the left-hand side of I is attributed to noise effects, which become important at low rf power. The deviation to the right-hand side of II is associated with the saturation effect in Fig. 2.

one-point fit of Eq. (4) to the experimental points for the following values of the parameters: $T_i = 0.5$ eV $\approx 2T_e$, $v_d/v_{Te} = 0.16$, and $k_z = m\pi/L = 0.16$ cm^{-1}. It is found that $m = 3$ is the only value that can be fitted to the experimental data with reasonable values of T_i and v_d. For $m > 3$ the mode is prevented from growing by ion-cyclotron damping and for $m < 3$ by electron Landau damping.

In interpreting Fig. 3 we note that the experimental function $A_0 = A_0(\Delta\omega)$ corresponds to a damping increment of 10 db (power) for a 0.4% change in frequency, indicating that it is caused by a damping mechanism which is an extremely sensitive function of frequency, identified here as the ion-cyclotron damping described by the third term in Eq. (4). This interpretation is supported by considering the experimental procedure described here. With $P_{rf} = 0$, the current is increased slightly beyond onset, in which case v_d is increased from $v_d < v_\Phi$ to $v_d > v_\Phi$. Under these conditions the data used to plot the curve in Fig. 3 show that the electron-drift growth term is about 10% larger than the electron Landau damping term. The growth rate is then positive and the instability grows until nonlinear saturation occurs. Under these conditions the frequency is given by Eq. (4) with $E_{rf} = 0$, and the ion-cyclotron damping is negligible. With $P_{rf} > 0$, the frequency is shifted downward so that the ion-cyclotron damping term reaches 7% of the drift term when P_{rf} reaches 60 mW, while the other two terms remain virtually unchanged, to reduce the growth rate sharply. Finally, since little of the coil power flow is dissipated (coil $Q \simeq 100$), the maximum power input to the plasma neglecting resistive losses in the coil is (60 mW/Q) or 0.6 mW. This sets an upper bound on lower-hybrid power flow, $(\pi R^2 E_\Omega^2/8\pi)v_g$, where $v_g \cong \Omega/K_z$, so that $E_{\|\Omega} = (K_z/K)E_\Omega \simeq 9.2\times 10^{-5}$ esu. Equation (4) predicts a downward frequency shift of ~ 1% for the instability at this field, in rough agreement with observations.

This work has been supported by the National Science Foundation Grant No. ENG-76-04635, U. S. Air Force Office of Scientific Research Grant No. 76-3129, and the U. S. Department of Energy. We thank C. R. Hall for his assistance.

---

[a]Permanent address: Dickinson College, Carlisle, Penna. 17013.

[b]Deceased.

[1]Ya. B. Fainberg and V. D. Shapiro, Zh. Eksp. Teor. Fiz. 52, 293 (1966) [Sov. Phys. JETP 25, 189 (1967)].

[2]M. Okamoto, T. Amano, and K. Kitao, J. Phys. Soc. Jpn. 29, 1041 (1970).

[3]A. K. Sundaram and P. K. Kaw, Nucl. Fusion 13, 901 (1973).

[4]R. Gore and H. Lashinsky, Phys. Fluids 22, 2178 (1979).

[5]A. Gelb and W. E. Vander Velde, *Multiple-Input Describing Functions and Nonlinear System Design* (McGraw-Hill, New York, 1968).

[6]R. Gore, J. Grun, and H. Lashinsky, Phys. Rev. Lett. 40, 1140 (1978).

[7]W. E. Drummond and M. N. Rosenbluth, Phys. Fluids 5, 150, 1507 (1962).

[8]N. D'Angelo and R. W. Motley, Phys. Fluids 5, 633 (1962).

[9]D. L. Correll, N. Rynn, and H. Böhmer, Phys. Fluids 18, 1800 (1975).

[10]M. Yamada and H. W. Hendel, Phys. Fluids 21, 1978 (1955).

[11]TFR Group, Phys. Rev. Lett. 41, 113 (1978).

[12]F. S. Mozer *et al.*, Phys. Rev. Lett. 38, 292 (1977).

[13]C. S. Liu and P. K. Kaw, in *Advances in Plasma Physics*, edited by A. Simon and W. B. Thompson (Wiley, New York, 1976), Vol. 6, p. 83.

[14]C. S. Liu and V. K. Tripathi, to be published.

[15]P. K. Kaw, in *Advances in Plasma Physics*, edited by A. Simon and W. B. Thompson (Wiley, New York, 1976), Vol. 6, p. 179.

[16]H. Lashinsky, in *Nonlinear Effects in Plasmas*, edited by G. Kalman and M. Feix (Gordon and Breach, New York, 1969), p. 451.

[17]H. Lashinsky and R. E. Monblatt, Rev. Sci. Instrum. 42, 1413 (1971).

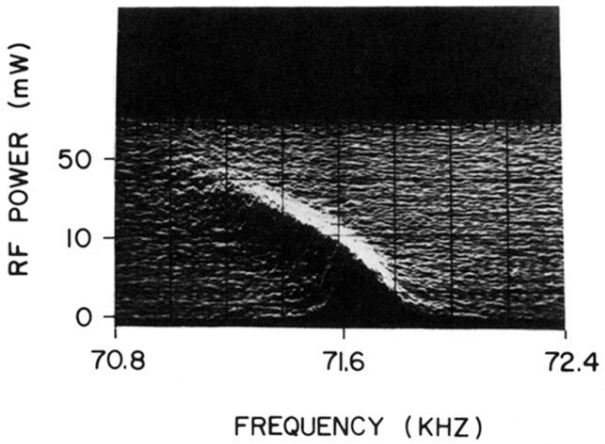

FIG. 1. Raster display (Ref. 17) showing the reduction of the frequency and amplitude of the current-driven ion-cyclotron instability caused by the application of radio-frequency power in the lower-hybrid range of frequencies. The instability signal is derived from fluctuations in the current to the endplate.